Adaptive actuator disc implementation for wind farm conditions

Gonzalo P. Navarro[a,b], A. Celeste Saulo[a,c], Alejandro D. Otero[d,b]

[a] *Facultad de Exactas y Ciencias Naturales, Universidad de Buenos Aires*
[b] *Centro de Simulación Computacional, CSC - CONICET*
[c] *Servicio Meteorológico Nacional, SMN - CONICET*
[d] *Facultad de Ingeniería, Universidad de Buenos Aires*

Abstract

The turbine wake simulation is important to understand the wind farm turbines interaction. This phenomenon involves a speed losses and turbulence injection effect, which can greatly affect the turbines downstream. The capability of the actuator turbine model to adapt its interference to the local wind condition on the rotation plane, is essential for the correctly downstream wake transference. In this work, the actuator disc model is improved, in order to make the thrust distribution on the disc depending on the local condition on its cells, and the orientation according to the incoming wind direction. OpenFOAM free software is used, with the ability to be run in parallel, using a stationary solution solver. This model is validated firstly with wind tunnel experiments available in literature, where one or two turbines are tested interacting with each other, and secondly with single wake measurements from a field campaign downwind industrial size turbines. Finally, a wind farm case is presented, in which the complex interaction of the turbines is tested for directions of low and high wake impact. The results show that this actuator disc improvement arrive to a better solution for wake interaction cases and its utility to obtain the wind farm power output for many directions at lower computational cost.

Keywords: actuator disc model, wind farms, wake interference, computational fluid dynamics

1. introduction

The wind energy production depends directly on inflow weather conditions, as well as the turbine sitting in wind farms. This last characteristic is important for turbine flow interaction, generating the wake effect, as explained by Politis et al. [1]. This phenomenon causes a speed reduction and an increase of the turbulence downstream of a turbine, affecting partially or totally the aerodynamics of turbines located downstream near the wake, with the consequent power losses.

The former analysis of wind turbines was originally developed by Betz and Glauert [2], among others, in the 1930s, based on the conceptual actuator model. This approximation allows to reduce the complexity of the problem, since the turbine is replaced by distributed forces that are exerted on the fluid, acting like a moment sink. In numerical solutions of the problem this approach allows the use of coarser meshes with good results, avoiding to reduce the mesh size to get good aerodynamic surface definition. Keck [3] summarizes the approaches for the location of the equivalent forces of the actuator model, with different levels of description and computational cost, depending whether a stationary or transient solution is sought. The simplest approach is the

actuator disc (AD) model, where forces are distributed all over the rotor area, is one of the most used in turbine modeling.

Within the AD family, two types of models can be implemented according to the equivalent forces distributed on the disc, as proposed by Wu and Porté-Agel [4]. In the standard AD model only the axial forces are included and distributed uniformly. If the characteristics of the blades are available, a more sophisticated AD model can be created, in which the axial and tangential forces are calculated and distributed radially according to the local characteristics of the blade. These two types of AD models are validated against boundary layer wind tunnel measurements in the reference, and it is found that the inclusion of the rotational forces improves the results in the near wake, while at further distances both models give similar results.

The validation of the AD models in wind farm scale is carried out, for example, by van der Laan et al. [5], in which meteorological mast and Lidar wake measurements for neutral boundary layer in three field campaigns are compared with computational results. The simulations are carried out using the AD model with axial and tangential forces distributed in the radial direction. In the far wake, measurements and simulations overlap on a bell shape. The application of the AD model to simulate the wake interaction effect is carried out by van der Laan et al. [6], comparing the measured and simulated power output deficit for different rows in two off-shore and one on-shore wind farms. The results show the sensitivity of the power deficit on the selection of the turbulence model and the negligible importance of including the rotation in the AD model. Wind farm simulations for an off-shore case is also presented by Castellani and Vignaroli [7], showing that the AD model is acceptable for complex flow over a large domain extension with changes of roughness between the sea and the neighboring islands covered with forest.

The AD model with only axial forces is the only feasible actuator model to implement using the standard data reported by turbine manufacturers, i. e. power and thrust curves (or the respective coefficients) in terms of the unperturbed wind speed. One drawback of this model is the incompatibility between the approximation of axial forces uniformly distributed and the wake interaction effect into a wind farm. This generates a non-uniform distribution of the incident velocity on the turbine rotor plane. For a more realistic simulation with the AD model, but keeping its simplicity, it is necessary to incorporate the axial force adaption to the local wind condition on the disc. This will allow to represent the overall interaction of wind farm turbines more precisely.

In this work, an improved version of the actuator disc model is presented, in which the thrust distribution on the disc is made adaptable to the local wind condition, and the actuator orientation follows the inflow direction using the same domain mesh for all cases. This adaptive behavior is achieved by model calibration for different inflow conditions. Due to the domain extension for wind farm simulation, parallel computation is needed. OpenFOAM (Open Field Operation and Manipulation) software [8] [9] is selected for that purpose, with a steady-state solver corresponding to a time-averaged solution of the wake effect.

In section 2, improvements to the actuator disc model are developed starting from the classical model. Next, in section 3 the new actuator disc model is validated against wind tunnel experiments available in literature, where one or two turbines are tested interacting with each other. Also a validation is carried out with single wake measurements behind a real turbine in a wind farm, covering two cases at different distance an ambient turbulence intensity. The improved model is tested for a large wind farm in section 4, where a wind farm case is presented, in which the complex interaction of the turbines and terrain is tested for a wide range of directions. Finally, some conclusions and outlook for further work are drawn in section 5.

2. Computational model

In this section, we describe the components of the modeling strategy, mainly the fluid dynamic solver and the actuator model that represents the turbine effect on the flow. After summarizing the classical actuator disc implementation we present some modification to improve its capability to model complex wakes in a wind farm.

2.1. Fluid dynamic equations solver

In order to carry out the flow simulations, OpenFOAM software is used. This is a free and open source computational fluid dynamic (CFD) tool, which allows the user to modify it freely and extend its functionality. Within the most common uses, it provides numerical approximations to stationary and transient solutions of fluid flows, using the finite volume method in polyhedral unstructured meshes. It is programmed in `C++` and has the capability to be run in parallel, allowing to simulate complex cases with large number of cells in the domain.

Among the available solvers in OpenFOAM, `SimpleFOAM` for stationary solution is chosen. It is a typical first choice in OpenFOAM and uses the SIMPLE (Semi-Implicit Method of Pressure Linked Equations) algorithm by Patankar for steady state calculations [10]. It solves the incompressible Reynolds Averaged Navier Stokes (RANS) equations [11].

In RANS formulation it is necessary to close the equations using a turbulence model. In the simulation of wind tunnel experiments, the standard k - ε model [12] is widely used by other authors to simulate the wake effect in the experiments presented in 3. This is a first order and two equations model, based on the transport equations for turbulent kinetic energy, k, and its dissipation rate, ε.

In wind farm simulations, it is common to impose as the inlet condition a neutral atmospheric boundary layer (ABL) [13]. This neutral condition corresponds to the situation in which mechanical effects predominate over heat transmission effects [13, 14] and a logarithmic vertical velocity profile is adopted [15]. To simulate ABL conditions, it is demonstrated that the standard k - ε model is not capable to solve correctly the wake effect [5], since this model tends to over predict the eddy viscosity within flows with high mean shear rate or massive separation, ending with a fast wake recovery. To solve this problem, a modified k - ε model, know as Realizable k - ε model, is chosen [16]. This model has been previously used with stadard coeficients by [17], showing a good agreement with wake velocity measurements. This is due to the fact that this improved model introduce a new formulation of the dissipation rate equation, which is capable of solving detachment and re-circulations, and specifically, to enhance the prediction of wakes when using actuator disc models.

OpenFOAM software already has an implementation of boundary condition functions for ABL profile for velocity (`atmBoundaryLayerInletVelocity`), k (`atmBoundaryLayerInletK`) and ε (`atmBoundaryLayerInletEpsilon`), depending on a terrain roughness coefficient and the velocity vector at a specific height. OpenFOAM software also has an implementation of the actuator disc model, `actuationDiskSource`. This implementation was used as base-case for the improvements to the proposed model in this work.

2.2. Standard actuator disc

The actuator disc model is based on the momentum theory, which states the momentum conservation [18]. This theory parameterizes the thrust and torque, applying conservation in the linear and angular momentum equations for a control volume corresponding to an annular section tube through the turbine. In the actuator disc model, the rotor is simplified as a permeable

disc with distributed axial forces, which intensity is equivalent to the average thrust exerted by the turbine blades. With this procedure, the turbine is not explicitly modeled, but instead those distributed forces produce an equivalent momentum sink.

If the aero-dynamic characteristics along the whole blade were available, an actuator disc with axial and tangential forces could be developed [19]. According to Tzimas and Prospathopoulos [20], if the available information only includes general manufacture information, such as power curve and thrust coefficient, only the axial component of the thrust can be included in the disc model.

On the classical application of the one-dimensional momentum theory, the axial force T_{total} is uniformly distributed over the whole blade sweep area (i. e. rotor disc):

$$T_{total} = \frac{1}{2}\rho C_t U_\infty^2 A_d, \tag{1}$$

where A_d is the disc area, ρ the air density, U_∞ is the unperturbed upstream velocity, and C_t is the thrust coefficient for the undisturbed velocity . The total thrust is uniformly distributed in the disc cells volume:

$$T_{cell} = T_{total}\frac{V_{cell}}{V_{disc}}, \tag{2}$$

where V_{disc} is the volume of the cells that cover the rotor disc and V_{cell} is the volume of each of these cells.

Near the disc, the upstream velocity field has a strong variation. This generates an uncertainty on choosing the location of the point where U_∞ is probed. Figure 1 shows the model sensitiveness to the distance where $U_{ref} \approx U_\infty$ is sensed. Figure 1 (a) shows the different normalized velocity values measured at different distances upstream the turbine for a fixed unperturbed velocity, U_∞. It can be observed that, for distances closer than 2 diameters, the sensed velocity is significantly lower than the reference U_∞. This reduces the thrust applied to the fluid according to equation 1, and affects the resulting wake. The induction zone produced in front of wind turbines was studied by Niels and Raul [21] combining a CFD solver with the actuator disc model. Velocity profiles presented in that study are very similar to those shown in figure 1 (a). In figure 1 (b), the resulting wake velocities for probe distances 0.5, 1, and 2 rotor diameters upstream are shown. In this case, in order to isolate the effect of velocity variation alone, the velocity was chosen in a constant thrust coefficient zone, resulting in the same C_t at each probe distance. This effect could be even worse if thrust coefficient noticeably varied from one sensed velocity to the other.

2.3. Adaptive actuator disc

Upstream inhomogeneity correction

The formulation of the classical actuator disc in section 2.2 assumes an uniform and known unperturbed inflow velocity [22]. Thus, when the turbine is immersed in a complex wake flow there is a need of establishing an equivalent U_∞ from the velocities in the surroundings of the turbine disc which can be unequivocally measured. Among several proposals reported in the literature, one common practice is the methodology used for example by Politis et al. [1] and Avila et al. [17] to compute U_∞ from the velocity through the disc U_d. Defining the axial induction factor as:

$$a = \frac{U_\infty - U_d}{U_\infty}, \tag{3}$$

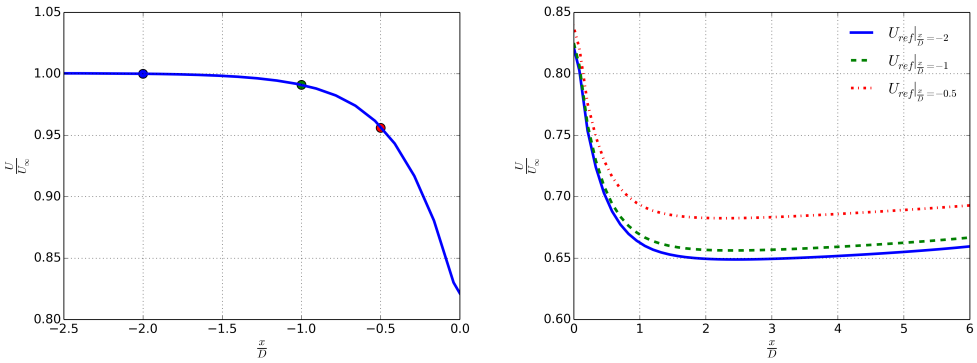

(a) (b)

Figure 1: Sensitivity of the wake to the distance where the reference velocity is measured. (a) Sample probes at three different upstream locations and (b) the corresponding normalized wake velocities.

and using results from the one-dimensional Betz theory and an empirical turbulent wake state relation [18], the thrust coefficient, C_t, and the axial induction factor a are related as,

$$C_t = \begin{cases} 4a(1-a) & a < 0.4, \\ 0.89 - \frac{0.20-(a-0.143)^2}{0.643} & a \geq 0.4. \end{cases} \tag{4}$$

Thus, U_∞ is computed iteratively from equations 3 and 4.

On the other hand, in the OpenFOAM actuator disc implementation another formulation to obtain the axial induction factor is chosen, using a relation between C_t and the power coefficient, C_p, deduced from the Betz theory and without the need to carry out an iterative process:

$$a = 1 - \frac{C_p}{C_t}. \tag{5}$$

In both methods, the fictitious unperturbed velocity could result in a turbine effect on the flow differing from the actual one because its computation inherits the limits of the Betz theory. Furthermore, the method in OpenFOAM not even accounts for the turbulent wake state correction making it usable for $a \geq 0.4 - 0.5$.

In order to test both methodologies of computing the thrust, we used the combination of the actuator model in section 2.2 with the CFD solver of section 2.1 in a setting similar to the wind tunnel experiment presented by Krogstad and Eriksen [23] (more details are given bellow in section 3.2). We imposed a known uniform unperturbed wind velocity as input boundary condition far enough from the actuator, with the corresponding thrust applied to it based on the C_t coefficient for that velocity. Then, we measured the wind velocity through the actuator disc U_d, and computed the induction factors resulting from this CFD simulation and from equations 4 and 5. The corresponding unperturbed velocity was computed from each induction factor, and the error with respect to the CFD disc velocity, ε_{U_∞}, was obtained. Table 1 compares results for those induction factors and unperturbed velocity errors for three different tip speed ratios (TSR). As can be seen, there are remarkable differences between both methods and the simulation, that could lead to errors in the thrust applied to the flow and the disc velocity, specially far from the optimum operation point corresponding to $TSR = 6$.

TSR	C_p	C_t	CFD		Equation (3)		Equation (5)	
			U_d/U_∞	a	a	ε_{U_∞}	a	ε_{U_∞}
3	0.12	0.40	0.896	0.104	0.113	1.2 %	0.700	198%
6	0.46	0.87	0.748	0.252	0.320	10 %	0.471	41%
10	0.16	1.07	0.673	0.329	0.705	128 %	0.850	348%

Table 1: Comparison between induction factors resulting from the CFD simulation and equations 4 and 5. For the two methods based on the Betz theory, the errors in computing the unperturbed wind velocity are also shown.

To avoid this problem, another method is used in this work to obtain a representative U_∞ from U_d. In this methodology, also used in [24], a single turbine is simulated for a wide range of known U_∞, imposing the respective C_t, and measuring the resulting velocity on the disc, U_d. This calibration process yields a relation $\overline{U}_\infty = f(U_d)$ used in this implementation to overcome the uncertainty in the determination the unperturbed velocity upstream. Thus, at each solution step the value of U_d is measured and, depending on this, both values of $\overline{U}_\infty$ and $\overline{C_t}$ are obtained corresponding to the thrust calculation from equation 1:

$$T_{total} = \frac{1}{2}\rho\overline{C_t}\,\overline{U}_\infty^2 A_d \tag{6}$$

with

$$\overline{C_t} = C_t(\overline{U}_\infty). \tag{7}$$

In-plane inhomogeneity correction

The reparameterization of the thrust and power curves described above aims to solve the problem of flow inhomogeneity upstream the turbine location. Another problem that appears in multiple wake flows is the inhomogeneity on the rotor disc manifested as variable wind speed at different locations of the turbine plane. This is characteristic in wind farm flow due to the interaction of wakes of several turbines. Thus, the actuator disc model needs to be modified in order to adapt thrust forces to the local condition on the disc, being able to capture U_d variations due to non-uniform inflow.

For a given turbine, the thrust coefficient at a particular working condition only depends on the geometrical setting of the blades, e. g. the pitch angle φ, and the TSR λ, which encompasses the unperturbed wind speed U_∞ and the rotor angular velocity ω,

$$C_t = C_t\left(\varphi, \frac{\omega R}{U_\infty}\right) = C_t\left(\varphi, \omega, U_\infty\right). \tag{8}$$

When a turbine is subjected to variable conditions on the rotor disc it adopts a particular reference setting imposed by its control system, but in some regions the blades work in off-design conditions. An off-design operating condition could be approximated by means of a Taylor expansion of C_t around a particular configuration defined by the pitch angle $\widetilde{\varphi}$, rotor angular velocity $\widetilde{\omega}$ and unperturbed wind speed $\widetilde{U}_\infty$ adopted as reference

$$C_t\left(\varphi, \omega, U_\infty\right) = \widetilde{C_t} + \frac{\widetilde{\partial C_t}}{\partial\varphi}\left(\varphi - \widetilde{\varphi}\right) + \frac{\widetilde{\partial C_t}}{\partial\lambda}\left[\frac{\widetilde{\partial\lambda}}{\partial\omega}\left(\omega - \widetilde{\omega}\right) + \frac{\widetilde{\partial\lambda}}{\partial U_\infty}\left(U_\infty - \widetilde{U}_\infty\right)\right] + \ldots \tag{9}$$

where quantities with a tilde are evaluated at the particular configuration, e. g. $\widetilde{C_t} = C_t|_{\left(\widetilde{\varphi},\widetilde{\omega},\widetilde{U}_\infty\right)}$.

Equation 9 clearly shows that to get an approximation to first order, the dependency of C_t with λ and φ must be known, or at least its first derivatives.

For a typical variable-pitch variable-speed turbine, roughly two working regions can be identified: below rated wind speed the turbine works at almost constant TSR with fixed pitch angle, and above rated and below cut-off speed it works with variable pitch angle and constant angular velocity resulting in variable TSR. The usual information provided by turbine manufacturers consist of the curve of thrust against wind speed, from which not even a nominal C_t–λ curve can be extracted. Off-design curves are seldom available for research prototypes and nonexistent for commercial turbines, such that the best one can approach with manufacturers commercial information is up to the first term of equation 9, which can be thought as a zero-order approximation to the C_t in off-design conditions. For different turbine control schemes similar problems arise.

In this work we propose a methodology, that we call *adaptive actuator disc*, in order to take into account for non-uniform inflow which is described below. This methodology adopts the C_t approximation mentioned above. Considering the group of cells that enclose the actuator disc, the CFD solver mentioned in section 2.1 gives one representative velocity in each cell i which is adopted as disc velocity U_{d_i} for that cell. From this velocity a corresponding unperturbed velocity $\overline{U}_{\infty_i}$ is obtained with the method described above. The thrust coefficient is defined in terms of equation 9, according to the operational setting of the turbine. If only the manufacturer data is available, a $\overline{C_t}$ is selected corresponding to the U_d at the rotor center which is considered the reference for the entire disc. Thus, the thrust applied by the turbine to the fluid in cell i is computed as

$$T_i = \frac{\frac{1}{2}\rho\overline{C_t}\,\overline{U}^2_{\infty_i} A_d V_i}{V_{disc}}. \tag{10}$$

with V_i, the volume of cell i and $V_{disc} = \sum_i V_i$. This requires that the U_d probe be performed for all cells that enclose the turbine rotor. Finally, the total thrust exerted by the turbine is

$$T_{total} = \sum_i T_i. \tag{11}$$

Power contribution for off-design parts of the turbine can be analyzed analogously as done previously for thrust force adopting a zero-order approximation if only the commercial power versus wind speed curve is available. Computing $\overline{C_p}$ similarly as before for $\overline{C_t}$, the power contribution of cell i is computed as

$$P_i = \frac{\frac{1}{2}\rho\overline{C_p}\,\overline{U}^3_{\infty_i} A_d V_i}{V_{total}}. \tag{12}$$

In order to obtain turbine power output, all power contributions are totalized as

$$P_{total} = \sum_i P_i. \tag{13}$$

This improved *adaptive actuator disc* implementation will be contrasted in the validation section 3, with what we will call *Uniform AD with calculated thrust*, implemented in [24], where U_d is computed as the average in the rotor disc and considered to be the velocity in all disc cells. Thus a uniform thrust is applied on the entire disc, with U_∞ and C_t obtained from that velocity. In some cases where the measured thrust is know, we also compare results for an AD with that thrust imposed (not computed), we call that implementation *Uniform AD with measured thrust*.

Orientation correction

As turbines orient their rotors facing the wind, when simulating cases with different wind directions, there are two possibilities for meshing the domain and locate the actuator discs. The one more frequently adopted is to keep the disc orientation and flow direction aligned with the mesh. This requires a different mesh for each inflow condition. As some examples, in [25] the entire domain mesh is built again for each direction, while in the methodology presented in [17] only the mesh surrounding the actuator disc is reconstructed. A different way of meshing, which was adopted in this work, is to keep the mesh fixed and rotate velocity vectors in border conditions and orient the discs according to the wind condition. This allows to save the meshing time for each case, which represents, for the stationary cases carried out in this work, approximately 25 % of the time to solve a single case. This time saving is significant and this methodology also paves the way for future transient simulations.

Using the same fixed mesh for all directions requires changing the disc cell selection criteria. In order to describe the disc as best as possible for any oblique direction, greater mesh density is required and cells are selected as belonging to the disc if their barycenter is located closer than a given tolerance from the ideal disc plane. The mesh has a fixed orientation, for example aligned with the north-south and east-west directions. As the wind can blow from any horizontal direction, the vertical boundary conditions faces can have either of two types: inflow or outflow. Each face is set with inflow boundary condition type if the projection of the wind speed on the face normal points inside the domain. Conversely, if that projection points outside the face it is set with outflow boundary conditions.

To test problem sensitiveness to cell size at disc location, we compared the results for different directions with those of the mesh aligned with the inflow. The mesh is composed by hexahedral cells with equal size Δ in the three directions near the disc, and mesh density is reported as the number of cell layers across the disc. The direction of the inflow was varied in a range of 180°, and the disc thickness was fixed equal to 0.15D. This way, for higher mesh densities, more cell layers will be contained in the volume of the disc. Two tests are reported herein, firstly a direct comparison between the velocity through the disc and secondly the resulting thrust in each case. We consider the latter as a highly representative measure, encompassing errors both in C_t and U_d, that given the square dependence on the velocity also prevents some kind of error compensation.

The simulations were carried on for an individual turbine in an open domain. For the velocity test, in each inflow direction the same T_{total} corresponding to the inflow velocity was equally distributed on the disc cells. The velocity was uniformly sampled on a fixed number of points, n, on a horizontal line along the disc diameter, and the root-mean-square of the error ($RMSE$) between the samplings corresponding to the flow misaligned with the mesh, U_{d_i}, with respect to the aligned one, U_{ref_i}, was computed as

$$RMSE = \sqrt{\frac{1}{n}\sum_{i=1}^{n}(U_{d_i} - U_{ref_i})^2}. \tag{14}$$

Figure 2a shows velocity errors normalized with the mean velocity, in terms of the inflow direction for different meshes with one, two and three layers of cells across disc thickness, corresponding to cell sizes Δ giving $\frac{D}{\Delta} = 7$, 14 and 21. It can be observed that the maximum relative $RMSE$ gets lower when the mesh is refined, from 8 % for the one-layer mesh to 3.4 % and 1.8 % when mesh density is increased to two and three-layer meshes, respectively. The second test performed on the orientation correction methodology is based on the computation of the disc thrust as a comprehensive variable as stated above. In this case, the adaptive actuator disc is located

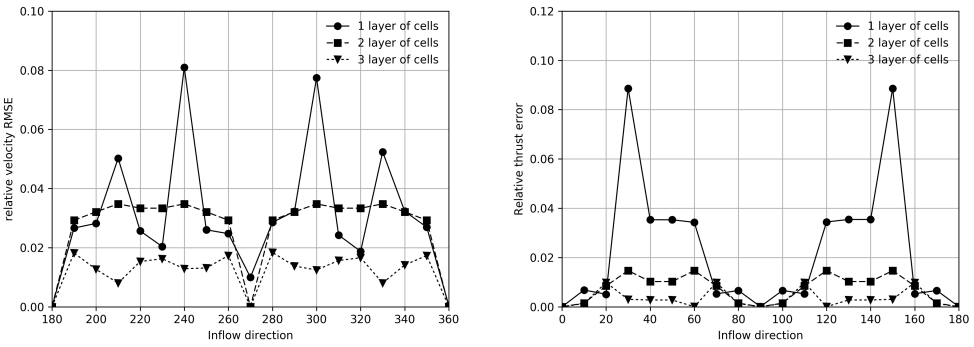

(a) (b)

Figure 2: Relative $RMSE$ in velocity on the disc (a), and relative error in thrust computation (b), for different discretizations depending on the inflow direction.

on a fixed mesh with different inflow directions and let to self align. The thrust is computed and contrasted against the value resulting when the inflow is parallel to mesh orientation. Results are shown for the three mesh densities with respect to wind direction in figure 2b. The behavior observed for the velocity is resembled in this case, more dense mesh reduce the relative error and fluctuations. Thrust maximum error reduces from 8.8 % in the one-layer mesh to 1.4 % and 0.9 % for two- and three-layer meshes. The two-layer mesh shows a maximum relative error quite uniform and lower than 4 % for the velocity and less than 2 % for the thrust as agregated quantity. Regarding the increment in computational cost associated to mesh refinement and this acceptable level of error this was the mesh density selected for other experiments in the present work.

3. Validation

In this section, the behavior of the adaptive actuator disc will be validated against field and wind tunnel measurements. Precise and consistent real data is scarcely found in the literature, two remarkable exception being the measurements at the *ECN Wind Turbine Test Site Wieringermeer* described by Schepers et al. [26] and the *Blind Test series* conduced by the Norwegian University of Science and Technology and published by Krogstad and Eriksen [23], Pierella et al. [27] and Krogstad et al. [28]. The data from the three *Blind Tests*, comes from the averaging of wind tunnel measurements of a scaled turbine. Thus, it shows a dependency of variables with the position from the center. Neither the adaptive AD nor the uniform AD can capture this variation. Moreover, the experimental origin of the data makes this variation non smooth. Another clear known source of mismatch between measurements and simulations is the marked asymmetry observed in the results, which is attributted by the authors to the presence of the tower which combines with wake rotation to render the results non symmetric. All in all, they make one of the more valuables sets of experimental data with which to compare. In the following, the implementation described in section 2 will be used to reproduce the working conditions of those situations. For wind tunnel measurements the standard k - ε turbulence model is chosen, due to the good results achieved by other authors in the *Blind Test series*. For the ABL simulations

the Realizable k - ε model with standard coefficients is used, because using the standard k - ε model in this cases leads to a weak wake comparing with field measurements, as is explained in section 2.1.

3.1. Single turbine wake - Field measurements

In order to evaluate the wake produced by the adaptive AD and the domain configuration adopted for ABL simulations, we use the wind measurements within single wakes from the *ECN Wind Turbine Test Site Wieringermeer*, previously used to compare with simulations by van der Laan et al. [5]. The portion of the wind farm to be simulated consists of two 2.5 MW Nordex N80 wind turbines, with 80 m of diameter and hub height, and a meteorological mast located in the vicinity of them.

From the measurements two particular cases are extracted. When the wind comes from direction 31°, called Eastern test case, the mast is immersed within the wake of one of the turbines located 2.5D far from it. The wind wake measurements are selected according to power output of the upstream turbine. A power range around 10.9 m/s is chosen, value that is taken as the hub height unperturbed velocity. In the simulation, the roughness coefficient, z_0, is set in order to obtain a value of the ambient turbulent intensity at hub height of 6 %, which is related to the unperturbed wind measurements from the eastern sector.

The other case simulated is called Western test case, in which for the direction 315° the wind mast is within the wake of the second turbine, at a longer distance of 3.5D. The wake measurements corresponding to the turbine power output range around 10.7 m/s are chosen. The z_0 is adjusted for a ambient turbulent intensity of 8 %, higher than the Eastern case due to the terrain roughness.

In figure 3 measurements and the corresponding simulations results are shown, with wake values centered in the reference wind direction, for the Eastern and Western cases. In both cases, the wakes obtained from the simulations are in good agreement with the measurements, presenting a slightly weaker wake in both cases. From these results it is expected that in the rest of the ABL simulations, the obtained power deficit due to wake interference will be slightly lower than the corresponding measurements.

3.2. Single turbine wake - Wind tunnel experiments (Blind test 1)

Since the adaptive actuator disc is derived from the uniform thrust approach, both must arrive at an equivalent result for uniform inflow conditions. In order to check this behavior, wind tunnel experiment *Blind Test 1* [23] is chosen as base case. The experimental setup is characterized by a single turbine of 0.90 m diameter and 0.80 m hub height. The turbine is located in a wind tunnel with dimensions 2.70 m wide, 1.80 m high and 11.15 m long. The inflow condition is set as $U_{ref} = 10m/s$ with low turbulence of 0.3 %. Among the different experimental tip speed ratio configurations, $TSR = 6$ is chosen for this comparison, corresponding an measured thrust coefficient of $C_t = 0.874$. This value was corrected in Pierella et al. [27] by eliminating the tower thrust. In the experiment, the wind speed at hub height and different transversal locations was measured at three distances from the turbine plane at 1, 3 and 5 rotor diameters downstream.

The same setup is simulated by means of the CFD solver of section 2.1 combined with both implementations of the actuator disc and compared with experimental results. Inflow boundary conditions, are set as an uniform U_{ref} in the front face, wall boundary condition are set at the sides, roof and floor, and outlet boundary conditions are set at the back. The mesh, is composed by two regions, the denser one close to the turbine and the other in the remaining of the tunnel

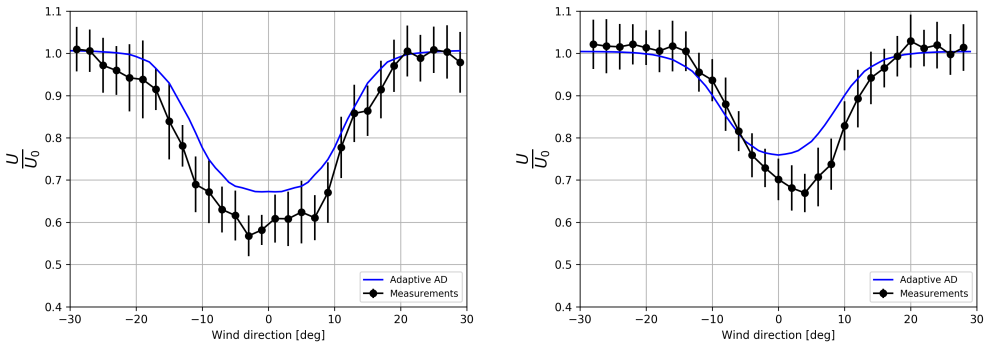

(a) (b)

Figure 3: Validation against Wieringermeer Eastern (a) and Western (b) test cases. Horizontal velocity profile at 2.5 (a) and 3.5 (b) diameters downstream. Comparison between measurements and simulations with the *Adaptive AD*.

domain. The mesh in the turbine region consists of a horizontal axis cylinder, centered on the turbine, with a diameter and thickness of $2D$. The near-turbine cell size is half the size of the tunnel mesh cells and approximately 0.07D. In this experiment, the k - ε turbulence model with standard coefficients is used.

In figure 4, simulation results are compared with the horizontal normalized measured velocity at different downstream locations. In addition, the horizontal velocity profile discrepancy between the standard and the adaptive actuator is calculated. Figures 4a to 4c contrast the wake profiles 1, 3 and 5 diameters downstream respectively.

Since the actuator disc model does not consider thrust variation due to blade geometry and local working condition, it becomes clear that the wake details, such as the speed recovery at turbine center, can not be captured near the disc, as seen in figure 4a and 4b. This phenomenon is due to the presence of the hub and the less active part of the blades that do not extend all the way to the axis, which is not detectable by the actuator disc with uniform thrust. The measured profile asymmetry is attributed by the experiment authors to the influence of the tower wake. In contrast, the resulting velocity profile from simulations, obtained with the actuator disc at one diameter distance, has a flat shape with rounded borders. At farther locations downstream, the simulated wake approaches a bell shape, which is closer to the measurements. In this way, the model errors are located in the center and borders of the disc, mainly for wake location close to turbine rotor. From this results it can be verified that this methodology correctly approximates the effect of the wind turbine in the medium range wake, adequately predicting the deficit amount and wake width. Comparing both actuator disc implementation from sections 2.2 and 2.3, in this case with uniform inflow velocity which defines a symmetric problem, give similar results with discrepancies in the order of 10^{-6} which make both curves indistinguishable.

3.3. Wakes of two aligned turbine - Wind tunnel experiments (Blind Test 2)

In order to test the model capability to capture the unknown uniform flow condition caused by an upstream turbine, the experiment presented in *Blind Test 2* publication [27] was used. It consists of two identical turbines in a tunnel similar to the one in *Blind Test 1*. The turbines are

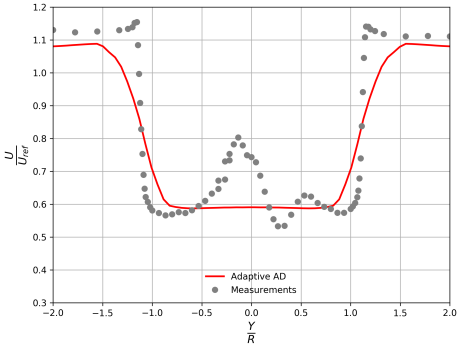

(a)

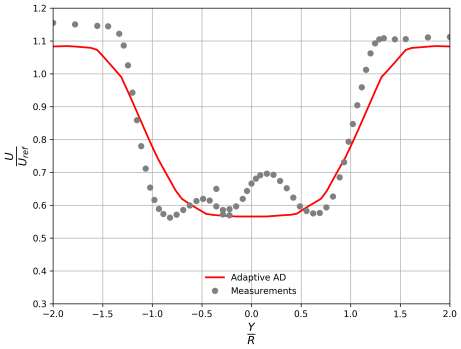

(b)

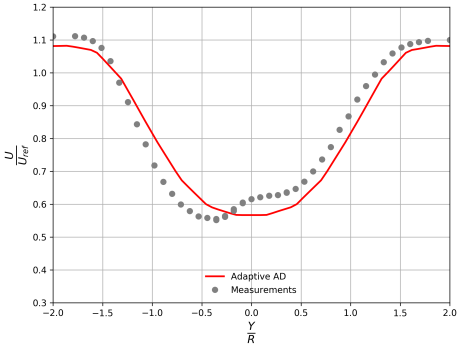

(c)

Figure 4: Validation against *Blind Test 1*. Horizontal velocity profile at 1 (a), 3 (b) and 5 (c) diameters downstream. Comparison between measurements and simulations with the *Adaptive AD*.

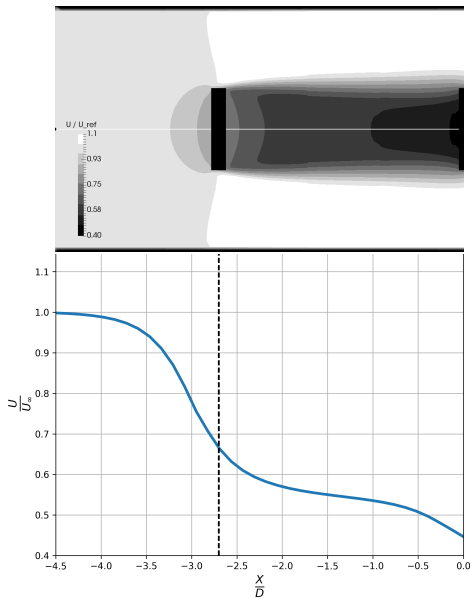

Figure 5: *Blind Test 2*: velocity field upstream the second turbine at turbine axis height (top), and velocity magnitude along second turbine axis line (bottom). The white line at top panel shows the axis line position.

located aligned with the flow direction, separated 3 diameters from each other. In this experimental setting, the upstream velocity field of the second turbine has a noticeable variation due to the interference of the first one resembling some typical wind farm working conditions. Figure 5 shows the longitudinal velocity profile upstream the second turbine. It can be seen that the velocity intensity is reduced when approaching the second turbine. This generates an uncertainty when choosing the location of the point where U_{ref} should be probed in the classical actuator disc methodology, as taking a U_{ref} near the disc generates a smaller thrust, with a consequent wake variation. This highlights the importance of the calibration process described in section 2.3.

As part of the experiment, the flow speed was measured at hub height, at different distances downstream from the second turbine. The experimental C_t value with respect to U_{ref} is 0.874 for the first turbine and 0.360 for the second one. When simulating this wake interference problem, the C_t in the second turbine is *a priori* unknown, since its value depends on the resulting velocity field at the second turbine disc. In order to apply the uniform thrust and adaptive actuator disc methodology, the value of C_t at different U_{ref} must be known. During he wind tunnel experimentation, the TSR were set to 6 for the first turbine and to 4 for the second, in order to set each one in the optimum working situation. As both turbines are similar, but each one is working at a different TSR, a C_t vs U_{ref} curve for each TSR was deducted from the known C_t vs TSR relation of the turbines, and used in the simulation. This procedure resulted in $C_t = 0.38$ for the simulations with both actuator disc methodologies, which can be taken as an additional cross-check of the methodology, as it differed from the experimental measurements in 5.5 %.

In figure 6a to 6c, the measured horizontal velocity profiles of *Blind Test 2* experiment and the simulation results using the adaptive actuator disc are compared. The figures correspond to sections 1, 2.5 and 4 diameters downstream. It can be observed that the model for the second turbine is able to solve the unknown incoming flow by means of the technique presented in

section 2.2. Compared with measurements, the error in the simulation is higher in the center and border of the disc, as for the one turbine case. Moving downstream from the turbine, the modeled wake gets closer to the measurements, reducing the average error of the velocity profiles. A good description of the amplitude and peak of the wake is achieved and as the wake develops its shape better resembles the measurements. Additionally, those results are compared in the figures with the wake resulting from applying the measured C_t in the uniform actuator disc model in order to evaluate the effect of this mismatch. The deviation in that case is only noticeable in the nearest section, revealing a good overall agreement.

3.4. Wakes of two shifted turbine - Wind tunnel experiments (Blind Test 3)

To test the capability of the adaptive actuator disc to simulate wakes of turbines not aligned, where the wakes of the upstream turbines impinge on the downstream turbine in an uneven way, *Blind Test 3*[28] experiment was reproduced. It consists of the same setting as the previous experiment, with the two turbines located with an offset of 0.44D normal to the flow. In this configuration, only half the wake of the first turbine impacts the disc of the second one, generating a non-uniform velocity field on the disc. This situation is shown in figure 7 where the velocity field on the cells of the second disc is plotted. In this case, only half the disc is affected by the first turbine wake, representing a case of local speed deficit, with a difference of 59 % between the extreme values. In the experiment, the first turbine is set to work at $TSR = 6$ and the second at $TSR = 4.75$ both with respect to U_{ref}. For this configuration, the C_t experimental values are 0.736 and 0.581 respectively.

In this experimental setting, the velocity field upstream the second turbine varies depending with the distance also, but in this case in a more complex way than in section 3.3 as both wake axis are not collinear. The variation of the axial velocity at different distances from the second disc is plotted in figure 8, where it is clearly seen that there is a lower speed region caused by the first turbine, followed by a recuperation zone given by the second turbine being out of the first one axis and lastly a deceleration due to the presence of the second turbine. Taking a U_∞ reference at different distances will cause different wake effects, again emphasizing the convenience of the method described in section 2.3.

As explained for the *Blind Test 2* case, the C_t value for the second turbine is *a priori* unknown and to arrive to the correct value, the velocity field over the second turbine need to closely represent the real situation. As in the previous test, C_t vs U_{ref} curves were constructed for both operating TSR. The simulation of this experiment with the uniform thrust actuator disc, resulted in a $C_t = 0.50$ for the second turbine, which represents an error of 13.8 % with respect to the experimental value. On the other hand, the simulation by means of the adaptive actuator disc, resulted in a $C_t = 0.53$, which better agree to the experimental value with an error of 8.6 %.

Figure 9 shows the comparison between measured and modeled velocity profile at different distances downstream the second turbine. It can be observed that the downstream wake from the second turbine is composed by the distant wake coming from the first turbine, which is weaker, with the addition of the closer and stronger wake from the second one. In comparison at 1D downstream, the measured wake transition between both wakes is pronounced, while the models describe smoother transitions. When the downstream distance increase to 3D, the transition in the measurements is more soft and the difference between the models and measurements is reduced.

Comparing the adaptive actuator disc with uniform actuator disc implementations it is seen, in figure 9a at closer distance from the second turbine, that the adaptive one closer describes the composed wake deficit while the uniform implementations overestimate the maximum deficit. At higher distance, shown in figure 9b, uniform models keep overpredicting the deficit although

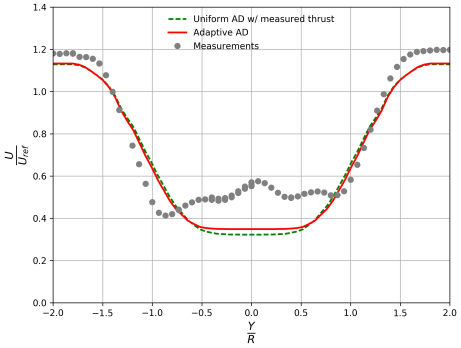

(a)

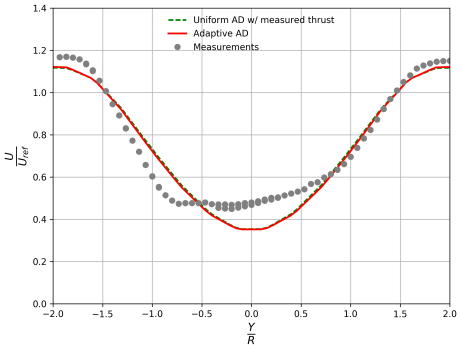

(b)

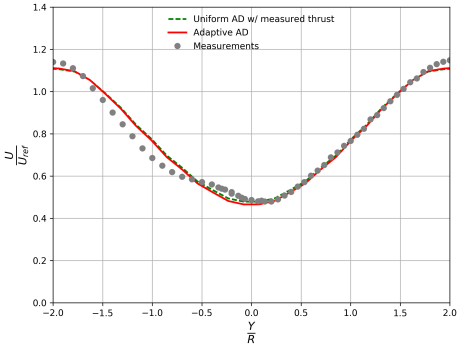

(c)

Figure 6: Validation against *Blind Test 2*. Horizontal velocity profile at 1 (a), 2.5 (b) and 4 (c) diameters downstream. Comparison between measurement and simulations using the *Adaptive AD* and the *Uniform AD with measured thrust*.

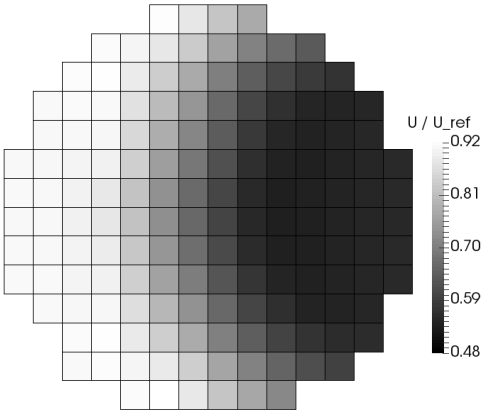

Figure 7: Velocity field on a plane in the center of the second disc.

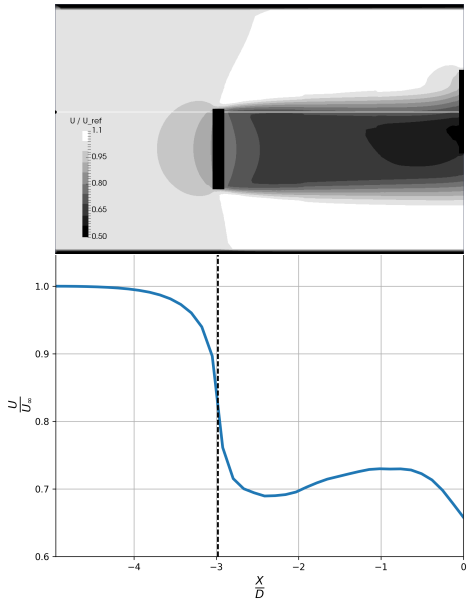

Figure 8: *Blind Test 3*: velocity field upstream the second turbine at turbine axis height (top), and velocity magnitude along second turbine axis line (bottom). The white line at top panel shows the axis line position.

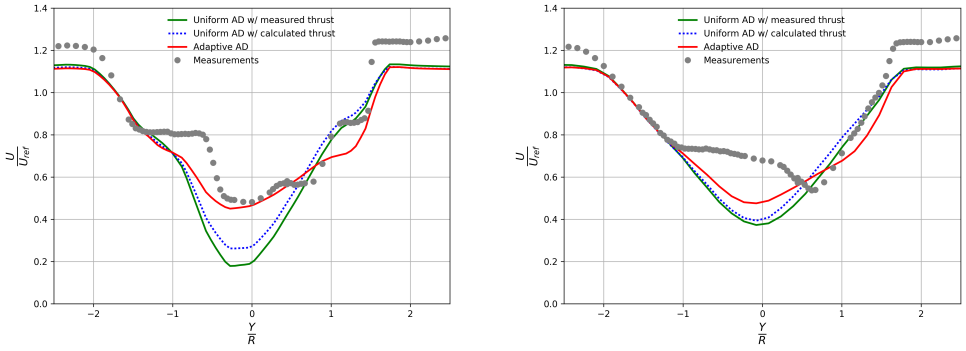

Figure 9: Validation against *Blind Test 3*. Horizontal velocity profile at 1 (a), and 3 (b) diameters downstream. Comparison between measurement and simulations using the *Adaptive AD*, and both *Uniform AD*.

all models get closer. In both cases it is seen that the strategy considering a uniform actuator fails to apply enough thrust to the region of the disc with higher speeds, overestimating the thrust for the region with lower speed. From this figures it is also seen that the uniform actuator disc with the thrust imposed according to the experimental C_t value gives a deficit larger than the experimental suggesting that the experimental value may be overpredicted.

4. Wind farm simulation

In this section we present results from the tools introduced above simulating turbine wake interference in a real utility-scale wind farm. The Rawson onshore wind farm is located in the Argentinean Patagonia, one of the windiest regions in the world, about 8 km inland. The studied configuration consisted of 43 turbines Vesta V90 1.8 MW with hub height of 80 m corresponding to stages I and II of the wind farm development. In December 2017, stage III began opertaing but it is not included in this study. The 43 turbines are distributed in 4 rows in the SW direction. The average turbine separation is 4D within each row and 12D between rows, giving the wind farm an approximate total extension of 4 km $\times$ 4 km. The manufacturer provides, as basic information on turbine performance, curves for the C_t, C_p, and power against U_∞. A meteorological mast is located in the NW corner 6D far from the nearest turbine, and the measurements are taken at hub height. Measured data is averaged over 10 min periods. Numerical results are compared with a set of 2 years data, which was cleaned up for missing data.

The computational domain is defined with clear margins added in all the edges, with the aim of allowing the development of the wake effect. A margin width of 7D was adopted, ending with total domain dimensions of 5.4 km $\times$ 5.2 km. On top of the farm, a clearance of 4.5D above the hub was adopted, giving a total height of 500 m from the mean ground level. Inflow border condition was defined corresponding to a neutral boundary layer and the the roughness coefficient is set in order to obtain an ambient turbulence intensity of 8 %, related to the average turbulence intensity measurements for all velocities in the unperturbed directions. Topography data was included to define the morphology of the ground where wall type boundary condition

was set. The terrain is almost flat in the domain extension, except for the southern turbines of the 1st and 4th rows, where differences up to 40 m compared with the rest of the turbines are present. The lateral walls of the computational domain are adjusted according to the incoming wind direction, as explained in section 2.3.

In order to make the turbine model adaptable to any velocity on the disc, and subsequently calculate the power output, the calibration instance of U_d in terms of U_∞ described in section 2 is carried out for a single turbine over the full range of operating velocities. The wind farm mesh is composed by two different regions. The background mesh has an increasing size in the vertical direction, from 1 m cells near ground surface expanding to 50 m at the top of the domain. This distribution allows to capture more details of the flow near the turbines and lower part of the atmospheric boundary layer. In addition, the local mesh around each turbine is defined as a vertical cylindrical region centered in the turbine, with diameter and height of 2D, and cell size according to the recommendations obtained from the mesh sensitiveness analysis reported in section 2. In this way, the cells located in the background mesh has about 12 m length, while within the cylinder enclosing each turbine disc, a minimum of 14 cells are placed along the diameter. In total, the domain reaches an amount of approximately 12 million cells, demanding a parallel computation for which the TUPAC cluster [29] hosted at the *CSC-CONICET* was used. 256 cores were used for the parallel resolution of each wind condition.

The analysis of the wind mast measurements reveals that the western quadrant winds prevails, with a higher frequency in the 270° direction. The mast is free of interference from the wind farm wake for inflow directions between 200° and 90°. This allows to use wind mast measurements to set the logarithmic profile of the inflow border condition and make comparisons with those cases. As an initial verification, power output of the nearest turbine to the wind mast and wind speed measured at the mast were compared with the manufacturer power curve, checking that both curves fit well.

In order to analyze different wake situations against measurements in this real wind farm, the four turbines nearest to the mast were selected as shown in figure 10. Three test cases were conducted based on this set of turbines for a reference velocity of 8 m/s, developing an analysis analogous to that of van der Laan et al. [30]. The simulations were run with this velocity set in the logarithmic profile boundary condition at hub height, and the measurements were selected in a range of 8 ± 1 m/s. As a mean of comparison we use the power efficiency [31], defined as the power ratio between two turbines, the first affected by the wake effect and the second receiving a clean inflow. This way we compare the complete simulation pipeline getting to the final quantity of interest. The numerical results correspond to simulations every 2° of direction within the studied range, in order to capture the wake effect for far turbines with a reasonable computational cost.

In the first test, the power loss of turbine 7 working inside the wake of turbine 8 is analyzed. This two turbines are aligned along direction 320° and separated by 4.7D. The interference phenomenon is analyzed for directions between 295° and 345°, with the maximum efficiency deficit at 320°. Figure 11a shows a comparison between simulation results and measurements, including uncertainty bars, for power efficiency between turbines 7 and 8. The deficit has a range of 30° with a maximum deficit of 43 %. In figure 11, results are shown in terms of the relative angle with respect to the reference direction, 320° in this first case.

For the other two test cases, three in-line turbines are selected, with turbines 7 and 6 in the wake of turbine 9. Turbine 7 and 6 are located 5.7D and 10.5D downwind turbine 9 along direction 25°. In this setting, wind directions from 0° to 55° are analyzed. In the second test, we compare the power efficiency of turbine 7 with respect to turbine 9. This case is similar to

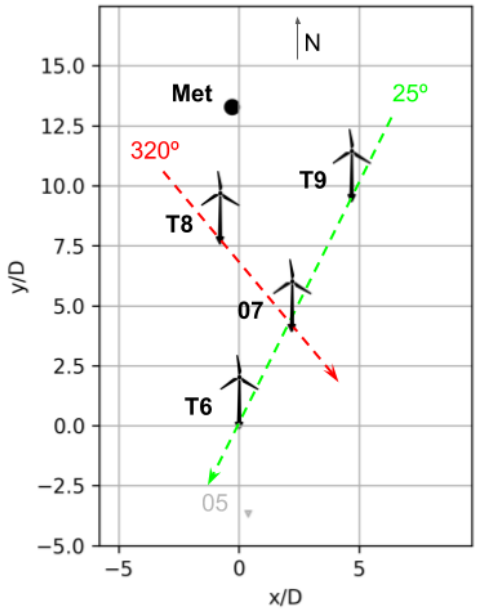

Figure 10: Four turbines selected and meteorological mast from the Rawson wind farm.

the former one considering turbines 9 and 8 but with the turbines more distant. The simulation result for this case are shown in figure 11b compared with the measurements. In this case, the interference is seen over a range of 25° which is smaller than in the previous case due to the larger distance between turbines, anyway the maximum deficit achieves a similar value. In the third test, the efficiency of turbine 6 with respect to turbine 9 was computed for the range of directions. The measurements show that turbine 6 is affected by the combined wakes of the two upstream turbines, resulting in wider a deficit range of 30° with a higher maximum deficit of 55 %.

Summarizing, simulations can accurately predict the deficit peaks in the three presented cases when compared with the measurements. The model correctly describes the peak and the development of deficit in the whole range of directions. In the third case a slightly less affection by the wakes in the extremes of the direction range related with wake superposition is noticed. Some discrepancies in direction where the maximum deficit is attained are observed that may be due to the Coriolis effect not considered in this model configuration, the turbines being not perfectly aligned along the reference direction, and/or the intrinsic uncertainties of the measurements. This direction discrepancy is also observed in other comparison between simulations and experiments.

Further analysis of the model capability to represent the wake effect in real wind farm situations is carried on in figure 12. Therein, the velocity modulus in the wind farm domain over a surface following terrain topography at hub height is shown. Figure 12a shows results for inflow direction of 270° corresponding to the most frequent sector, and velocity reference set at 8 m/s at hub height in the boundary conditions. The wind farm efficiency in this case is about 88.5 %

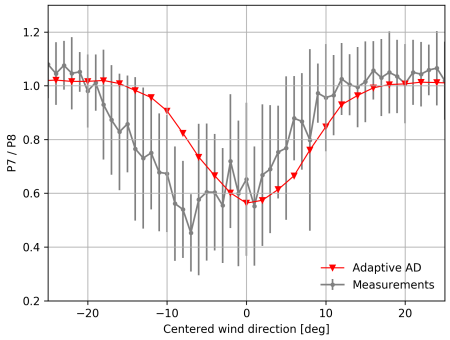

(a)

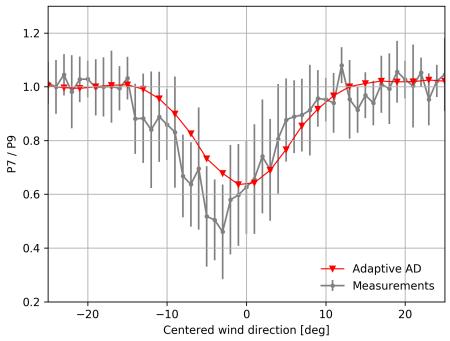

(b)

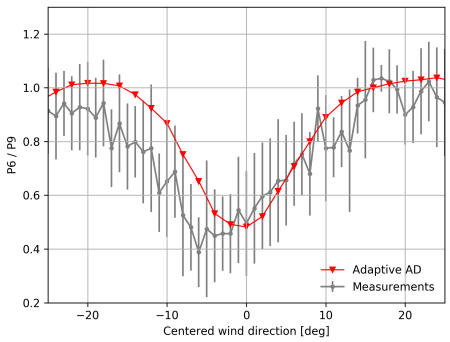

(c)

Figure 11: Modeled and measured power efficiency in terms of the relative wind direction for 8 m/s inflow velocity: (a) turbine 7 with respect to turbine 8 (reference wind direction 320°), (b) turbine 7 and (c) turbine 6 with respect to turbine 9 (both cases with reference direction 25°).

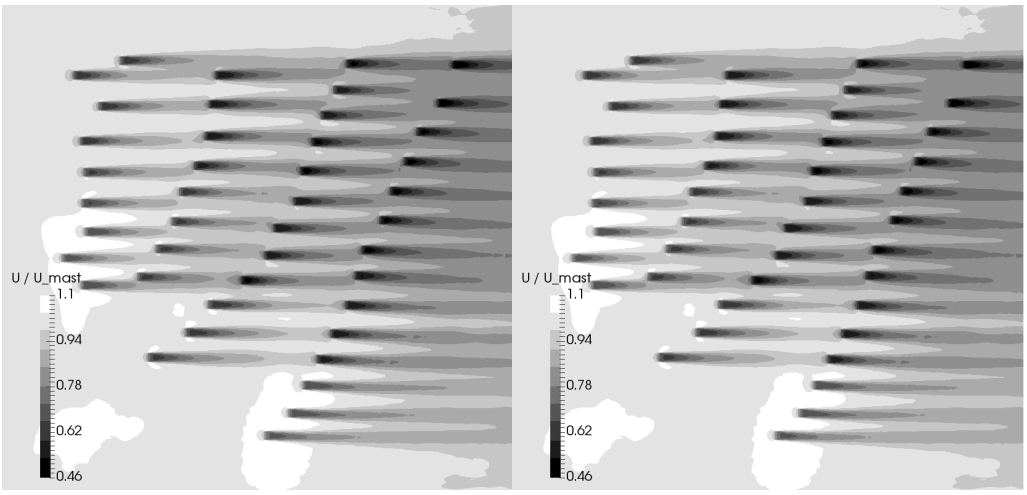

(a) (b)

Figure 12: Wind farm wakes at hub height for boundary condition reference inflow wind of 8 m/s for: (a) 270° and (b) 30° direction.

Direction	270°	30°
Measurements	86.0 %	73.7 %
Simulation	88.5 %	75.0 %

Table 2: Wind farm efficiency comparison between measurements and simulation for two representative inflow directions.

which can be clearly explained observing that wakes seldom interact with downstream turbines, with high speed channels forming between wakes that accelerate the flow impinging on turbines of following rows. Also, due to the large row separation, flow inside wakes is able to recover momentum before reaching the next row. Conversely, figure 12b shows analogous results for direction of 30° corresponding to the case with higher wake effect. In this case, wakes of several turbines in the same row align and result embedded one inside the others. This results in heavy interference as wakes of upstream turbines impinge the downstream ones without being able to recover much of their energy, due to the shorter turbine separation. In this case, wind farm efficiency is about 75.0 %. Table 2 shows a comparison between measurements and simulations in these two limiting cases with maximum and minimum wake interference effect.

falta figura 30 grados, se esta procesando

Figure 13 also shows the individual turbine power comparing simulation results and measurements. Mean power measurements filtered for a direction range of 270°±2.5° and meteorological mast velocity in the range 8±1 m/s are presented in figure 13a. Values are normalized against turbine power corresponding to the mast velocity. Those values serve as reference to evaluate the behavior of the model in this situation, which results are shown in figure 13b. The simulation was carried on with an inflow velocity at hub height of 8 m/s from 270°. The model accurately captures the terrain effect for the higher turbines (e. g. southern turbines of first and forth turbine rows) and the wake effect in the central part of the last two rows, while a slight mismatch is noticed in the prediction of some of the central and southern turbines of the second row. The

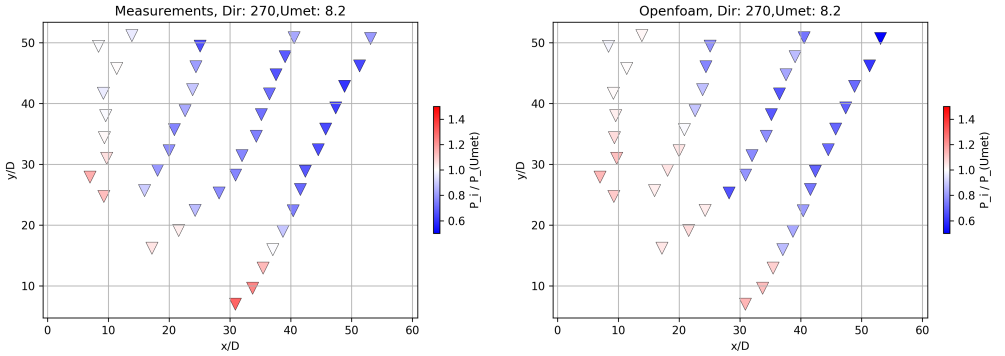

Figure 13: Comparison of individual turbine normalized power for reference inflow wind of 8.2 m/s and 270° direction at the wind mast: (a) measurements and (b) simulation.

overall power computed from the simulation is contrasted with measurements in table 2. In both cases, with low and high wake effect, the wind farm efficiency is well predicted. The minor differences may be explained regarding that the measurements comprises situations with different atmospheric stability conditions which have an effect on the power production.

5. Conclusions

In this work, an implementation of the actuator disc model adapted for wind farm conditions was presented. The main characteristics of this implementation are its capability to adjust the thrust and power when the inflow wind is not homogeneous in the rotor area, to self-orient according to local wind direction making it independent of the numerical mesh orientation, and to resolve the uncertainty in the upstream unperturbed velocity determination. This implementation improves the flow–turbine interaction, maintaining the restriction of using minimal turbine information as usually reported by the manufacturers, i. e. thrust and power (or the respective coefficients) against unperturbed flow speed. Special attention was put in a development based on open source tools, which due to the computing power requirements, could be executed in parallel high performance computers.

According to the results obtained from the simulations of wind tunnel cases, the adaptive AD achieves a good description of the far wake, both for a single and for two turbines in different layouts. The modification in the actuator disc formulation for the local trust estimation on a non-uniform inflow condition, improved the results in cases of local speed deficit on the turbine disc. The wind farm modeling in neutral ABL conditions was carried on using a unique mesh for all wind directions, since both border conditions and disc orientation could adapt to different inflow cases. The topography of the terrain was also included and its effect on a differential power production is clearly captured when analyzing the real wind farm case. Comparing with wind mast measurements from a single wake case, the results using the actuator disc shows good agreement with the measured wake, both for high and low ambient turbulence intensity. For wake interference between two and three turbines, the turbine power efficiency computed from

simulation results closely resembles that of measurements. The simulation of a full onshore utility scale wind farm shows excellent agreement both for low and high wake effect situations.

As a conclusion, despite being a very simple model, the adaptive AD achieves a correct description of the velocity deficit, both in shape and intensity, in complex wake and terrain situations. Thus, it is a convenient way for simulations of wind farm wakes, in which a general description is obtained at a feasible computational cost.

As an outlook for further work, we plan to focus our research efforts in the study of how more complex actuator models could improve wake description regarding the balance between computational cost, description level, and difficulty availability of turbine data required. Other topic that need further insight is how different ABL stability conditions affect the wind farm efficiency for different intensity of the wake effect. Also, the model set up presented herein opens several opportunities to study different phenomena that are indeed crucial for wind farm operation. For example, thanks to its ability to adapt to changing wind farm conditions, transient simulations of wind farm working condition, considering both changes in velocity and direction, could be simulated.

6. Acknowledgments

The authors acknowledge the financial support made available by the National Scientific and Technical Research Council through grant PIP 11220120100480CO; and the National Agency for Scientific and Technological Promotion through grant PICT2013-1338. The measurement data was kindly provided by GENNEIA S.A., for which the authors are very grateful. The authors would like to acknowledge the computational time from the TUPAC cluster made available by the *CSC-CONICET* for conducting this research.

References

[1] Politis, E.S., Prospathopoulos, J., Cabezon, D., Hansen, K.S., Chaviaropoulos, P., Barthelmie, R.J.. Modeling wake effects in large wind farms in complex terrain: the problem, the methods and the issues. Wind Energy 2012;15(1):161–182.

[2] Glauert, H.. Airplane propellers. In: Aerodynamic theory. Springer; 1935, p. 169–360.

[3] Keck, R.E.. A numerical investigation of nacelle anemometry for a HAWT using actuator disc and line models in CFX. Renewable energy 2012;48:72–84.

[4] Wu, Y.T., Porté-Agel, F.. Large-eddy simulation of wind-turbine wakes: evaluation of turbine parametrisations. Boundary-layer meteorology 2011;138(3):345–366.

[5] van der Laan, M.P., Sørensen, N.N., Réthoré, P.E., Mann, J., Kelly, M.C., Troldborg, N., et al. An improved k-ε model applied to a wind turbine wake in atmospheric turbulence. Wind Energy 2015;18(5):889–907.

[6] van der Laan, M.P., Sørensen, N.N., Réthoré, P.E., Mann, J., Kelly, M.C., Troldborg, N., et al. The k-ε-fp model applied to wind farms. Wind Energy 2015;18(12):2065–2084.

[7] Castellani, F., Vignaroli, A.. An application of the actuator disc model for wind turbine wakes calculations. Applied Energy 2013;101:432–440.

[8] Weller, H.G., Tabor, G., Jasak, H., Fureby, C.. A tensorial approach to computational continuum mechanics using object-oriented techniques. Computers in physics 1998;12(6):620–631.

[9] OpenFOAM. 2017. URL `http:/www.openfoam.org/`.

[10] Patankar, S.. Numerical heat transfer and fluid flow. CRC press; 1980.

[11] Durbin, P.A.. Turbulence closure models for computational fluid dynamics. Encyclopedia of Computational Mechanics 2004;.

[12] Launder, B.E., Spalding, D.B.. The numerical computation of turbulent flows. Computer methods in applied mechanics and engineering 1974;3(2):269–289.

[13] Panofsky, H.A., Dutton, J.. Atmospheric Turbulence: Models and Methods for Engineering Applications, 397 pp. John Wiley, New York; 1984.

[14] Stull, R.B.. An introduction to boundary layer meteorology; vol. 13. Springer Science & Business Media; 2012.
[15] Hargreaves, D., Wright, N.G.. On the use of the k–ε model in commercial CFD software to model the neutral atmospheric boundary layer. Journal of Wind Engineering and Industrial Aerodynamics 2007;95(5):355–369.
[16] Shih, T.H., Liou, W.W., Shabbir, A., Yang, Z., Zhu, J.. A new k - ε eddy viscosity model for high reynolds number turbulent flows. Computers & Fluids 1995;24(3):227–238.
[17] Avila, M., Gargallo-Peiró, A., Folch, A.. A cfd framework for offshore and onshore wind farm simulation. In: Journal of Physics: Conference Series; vol. 854. IOP Publishing; 2017, p. 012002.
[18] Burton, T.. Wind energy handbook. Wiley; 2001.
[19] Réthoré, P.E., Laan, P., Troldborg, N., Zahle, F., Sørensen, N.N.. Verification and validation of an actuator disc model. Wind Energy 2014;17(6):919–937.
[20] Tzimas, M., Prospathopoulos, J.. Wind turbine rotor simulation using the actuator disk and actuator line methods. In: Journal of Physics: Conference Series; vol. 753. IOP Publishing; 2016, p. 032056.
[21] Niels, T., Raul, M.A.. A simple model of the wind turbine induction zone derived from numerical simulations. Wind Energy ????;20(12):2011–2020. doi:10.1002/we.2137.
[22] Sanderse, B., Pijl, S., Koren, B.. Review of computational fluid dynamics for wind turbine wake aerodynamics. Wind energy 2011;14(7):799–819.
[23] Krogstad, P.Å., Eriksen, P.E.. "Blind test" calculations of the performance and wake development for a model wind turbine. Renewable energy 2013;50:325–333.
[24] van der Laan, M.P., Sørensen, N.N., Réthoré, P.E., Mann, J., Kelly, M.C., Troldborg, N.. The k-ε-fp model applied to double wind turbine wakes using different actuator disk force methods. Wind Energy 2015;18(12):2223–2240.
[25] Porté-Agel, F., Wu, Y.T., Chen, C.H.. A numerical study of the effects of wind direction on turbine wakes and power losses in a large wind farm. Energies 2013;6(10):5297–5313.
[26] Schepers, J.G., Obdam, T.S., Prospathopoulos, J.. Analysis of wake measurements from the ECN Wind Turbine Test Site Wieringermeer, EWTW. Wind Energy 2012;15(4):575–591.
[27] Pierella, F., Krogstad, P.Å., Sætran, L.. "Blind Test 2" calculations for two in-line model wind turbines where the downstream turbine operates at various rotational speeds. Renewable Energy 2014;70:62–77.
[28] Krogstad, P.Å., Sætran, L., Adaramola, M.S.. "Blind Test 3" calculations of the performance and wake development behind two in-line and offset model wind turbines. Journal of Fluids and Structures 2015;52:65–80.
[29] Vinazza, D., Otero, A., Soba, A., Mocskos, E.. Initial experiences from tupac supercomputer. In: Latin American High Performance Computing Conference. Springer; 2017, p. 38–52.
[30] van der Laan, P.M., Sørensen, N.N., Réthoré, P.E., Mann, J., Kelly, M.C., Troldborg, N., et al. The k-ε-fp model applied to wind farms. Wind Energy 2015;18(12).
[31] Nygaard, N.G.. Wakes in very large wind farms and the effect of neighbouring wind farms. In: Journal of Physics: Conference Series; vol. 524. IOP Publishing; 2014, p. 012162.